Proceedings of the 28th IEEE
EMBS Annual International Conference
New York City, USA, Aug 30-Sept 3, 2006

Intra-myocardial cusp waves and their manifestation in optical mapping signals

Olivier Bernus, Christian W. Zemlin, Arvydas Matiukas, Christopher J. Hyatt, and Arkady M. Pertsov

Abstract—**The rotating fiber orientation within the cardiac wall substantially affects the electrical propagation and can cause intra-myocardial cusp waves. Numerical simulations have shown that the cusps form in layers where propagation is perpendicular to the fiber orientation and lead to complex wave front morphologies. They can travel across layers and break through at the epi- or endocardial surfaces where they cause apparent accelerations of propagation. The validation of these results remains a major experimental challenge. In the present study, we investigate both computationally and experimentally how intramural cusp waves can be detected using optical imaging. Our simulations show that cusps alter the optical upstroke morphology and can be detected well before they reach the surface (up to 1 mm deep). Experiments in Langendorff-perfused guinea pig hearts are consistent with our numerical findings.**

I. Introduction

The cardiac muscle is well known to conduct action potentials anisotropically, showing a larger conduction velocity along than across muscle fibers [1]. The fiber orientation rotates throughout the myocardial wall up to 180°, depending on the species [2,3]. This has been termed rotational anisotropy and the rotation has often been assumed to have a linear dependence on depth throughout the bulk of the myocardial wall [2].

Rotational anisotropy substantially affects electrical propagation and repolarization in cardiac tissue [4,5]. Several studies showed that fiber rotation could produce intra-myocardial cusp waves and complex epicardial activation patterns resulting from cusps reaching the epicardium [6-9]. Recently, our group derived the equation for the asymptotic shape and velocity of wave fronts in anisotropic tissue [8]. This equation permits to predict the time and location where intra-myocardial cusps would reach the endo- or epicardial surface, a prediction that was verified numerically.

Fig.1 illustrates the formation of an intramural cusp wave. The left panel shows the intra-myocardial fiber orientation in four selected layers. The right panel shows isochrones of a wave front that was initiated at the $x = 0$ surface. Initially the wave front is planar. As the wave propagates to the right, a cusp forms in the layer where the fibers are perpendicular to the wave propagation (circle). With time, the cusp moves across fiber layers until it reaches the epicardium (white arrow), where it causes an apparent acceleration of propagation (less densely packed isochrones). Note also that the angle of the wave front with respect to the epicardium changes after the cusp has reached that surface.

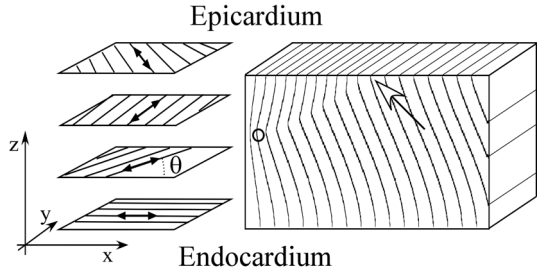

Fig.1. Fiber rotation in the myocardial wall and intra-myocardial cusp. The left panel shows the rotation of the fibers (arrows) from endo- to epicardium. The fiber orientation is defined by its angle θ with the x-axis. The right panel shows isochrones of a propagating wave initiated at the surface x=0. A cusp is formed in the layer where the fibers are perpendicular to the propagation direction (circle). The cusp eventually reaches the epicardium (white arrow), where it causes an apparent acceleration of the propagation (density of isochrones on epicardium decreases). Calculations were performed in a slab of 5 cm × 1 cm × 0.2 cm (vertical dimension is stretched for clarity) and isochrones are plotted at 5 ms intervals

In the present study, we assess the feasibility of detecting subsurface intra-myocardial cusp waves using optical imaging. Our group showed that the upstroke of the optical action potential contains information about the intra-myocardial wave front orientation [10][11]: if the wave front propagates "towards" the imaged surface, the upstroke will show a slow foot and reach maximal slope (denoted by V^*) at high levels, whereas the opposite is true for a wave front propagating "away" from the imaged surface (see Fig. 2). We hypothesize that any discontinuity in the wave front orientation will affect the optical upstroke if it occurs sufficiently close to the imaged surface. Here, we test our hypothesis both computationally and experimentally.

Manuscript received April 30, 2006. This work was supported in part by NIH Grants R01-HL071635 and R01-HL071762, and by a postdoctoral fellowship of the Research Foundation Flanders (O. Bernus).

O. Bernus is with the Department of Mathematical Physics and Astronomy, Ghent University, 9000 Ghent, Belgium, and with the Department of Pharmacology, SUNY Upstate Medical University, Syracuse, NY 13210 USA (e-mail: bernuso@upstate.edu).

C.W Zemlin, A. Matiukas and C.J. Hyatt are with the Department of Pharmacology, SUNY Upstate Medical University, Syracuse, NY 13210 USA (e-mails: zemlinc@upstate.edu, matiukaa@upstate.edu and hyatt_cj@hotmail.com).

A.M. Pertsov is with the Department of Pharmacology, SUNY Upstate Medical University, Syracuse, NY 13210 USA (e-mail: pertsova@upstate.edu, phone: 315-464-7986, fax: 315-464-8014).

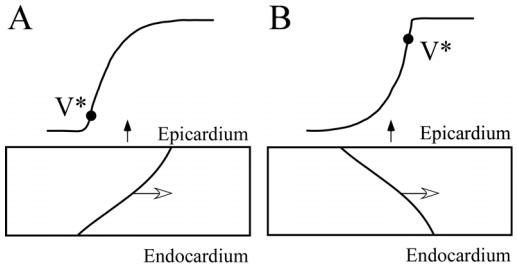

Fig.2. Optical upstroke morphology recorded from epicardium as a function of the direction of propagation. Panel A shows the optical upstroke for an electrical excitation wave propagating at a positive angle with the epicardial surface. The level *V** at which the maximal slope is reached, is close to the foot of the action potential. Panel B shows the optical upstroke for a wave propagating at a negative angle with the epicardium. In this case, the maximal slope is reached towards the end of the upstroke.

The general outline of this paper is as follows. First, we generate computational examples of intra-myocardial cusp waves. Next, optical action potentials of these cusp waves are calculated and their upstrokes are analyzed as a function of the cusp's depth. Finally, we present experimental results of intra-myocardial cusp waves and relate them to our theoretical findings.

II. Materials and Methods

A. Model of cardiac activity

The propagation of an action potential in myocardium is modeled by the following reaction-diffusion equation

$$\partial_t V_m(\vec{r},t) = - I_{ion}(\vec{r},t)/C_m + \nabla D \nabla V_m(\vec{r},t), \quad (1)$$

where V_m is the transmembrane potential, C_m is the membrane capacitance, $\vec{r}$ is the position vector, $D = \sigma/S_v C_m$ is the diffusivity tensor, with σ the conductivity tensor and S_v the surface-to-volume ratio of the cell. I_{ion} represents the total transmembrane ionic current. It was calculated using the latest variant of the dynamic Luo-Rudy model [12].

To integrate (1) we used an explicit scheme as described in [8] using a time step of 0.01 ms and a space step of 0.10 mm. Simulations were carried out on a parallel cluster consisting of 32 dual AMD Athlon MP2200+ processors running at 1.8 GHz.

B. Optical model

The light propagation in cardiac tissue is described by the time-independent diffusion equation [10,13]:

$$(3\mu_s' + 3\mu_a)^{-1} \cdot \nabla^2 \Phi(\vec{r}) - \mu_a \cdot \Phi(\vec{r}) + Q = 0, \quad (2)$$

where Φ is the photon density within the tissue due to an inclusion (source or sink) Q, μ_s' is the reduced scattering coefficient and μ_a is the photon absorption coefficient. We assumed Robin boundary conditions at all surfaces:

$$\Phi = l_s \cdot \nabla \Phi, \quad (3)$$

where l_s is the so-called extrapolation distance [14] and takes refractive index mismatches at the boundary into account.

The electrical (1) and optical (2) models were coupled through the source function Q in (2), to account for the voltage dependent fluorescence changes of the dyes [10,13]:

$$Q = \beta \cdot \Phi_{ex} \cdot V_m, \quad (4)$$

where β represents the quantum yield of the dye and Φ_{ex} is the local photon concentration of the excitation light.

Equation (2) was solved analytically by using the method of images [15,16]. The recorded surface distribution of voltage-dependent signals was calculated using Fick's law.

C. Model parameters

We simulated a three-dimensional slab of the myocardial wall representing a portion of the left ventricular wall of the guinea pig. We defined the z direction to be transmural from endo- to epicardium, and the x and y directions to be parallel with the endocardial surface (see Fig. 1). The slab's dimensions were 5 cm × 1 cm × 0.2 cm. The diffusivity tensor D was defined as in [17], to account for the anisotropic properties of cardiac tissue due to transmural fiber rotation. The diffusivity, D_L, in the longitudinal direction was 1 cm^2/s and in the transverse direction, D_T, was 0.11 cm^2/s. The transmural fiber rotation angle θ was assumed to be a linear function of the depth:

$$\theta(z) = k \cdot z + \theta_{endo}. \quad (5)$$

The rate of rotation k was set at 20°/mm [2].

Optical parameters were chosen for the widely used fluorescent dye DI-4ANEPPS [10,15]: μ_s'= 1.5 mm^{-1}, μ_a = 0.35 mm^{-1} and l_s = 0.8 mm for the excitation and μ_s'= 1.5 mm^{-1}, μ_a = 0.12 mm^{-1} and l_s = 1.0 mm for the emission.

D. Experiment

All experimental protocols conformed to the Guide for the Care and Use of Laboratory Animals and were approved by the Committee for the Humane Use of Animals of the SUNY Upstate Medical University. Guinea pigs (n=3) were isolated and Langendorff perfused with a standard oxygenated Tyrode's solution at 80 mm Hg and 36ºC (see [18] for details). The heart was continuously paced at the frequency of 3.3 Hz. Diacetyl-monoxime was added to the Tyrode's solution (15 mmol/l) to stop contractions. The preparation was stained by injecting 1 ml Ringer solution containing 10 nmol of the voltage-sensitive dye di-4-ANEPPS into the perfusion flow.

The optical setup was similar to the one described previously [18]. The video images, 20 mm in diameter area (80x80 pixels, 14bit), were acquired at 2000 frames per second. We used ensemble averaging to improve signal to noise ratio (i.e., averaging the optical signals from ~70 sequential recordings).

III. Results

A. Simulated intra-myocardial cusp waves

In order to study the manifestation of intra-myocardial cusp waves in optical signals, we generated several computational examples where the cusp breaks through at various distances, denoted by x_c, from the stimulation site.

This was achieved by varying the initial depth of the cusp through the parameter θ_{endo} in (5) [8].

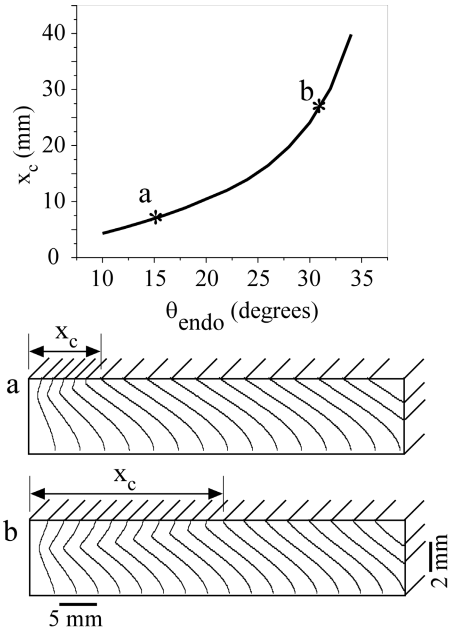

Fig. 3. Distance x_c of cusp breakthrough on epicardium as a function of the endocardial fiber orientation θ_{endo}. Transmural isochronal maps are shown for two values of θ_{endo}: 15° (a) and 30° (b). Isochrones are plotted at 5 ms intervals in a slab of 5 cm × 1 cm × 0.2 cm.

The plot in Fig. 3 shows how the distance x_c depends on θ_{endo}: the distance x_c increases as θ_{endo} increases, because the θ=90° layer gradually moves away from the epicardial surface. Transmural isochronal maps are shown for two selected values of θ_{endo}: in panel (a) the cusp is formed near the epicardial surface and breaks through at a distance x_c = 7.5 mm (θ_{endo} = 15°), whereas in panel (b) the cusp is formed deeper in the myocardial wall and reaches the epicardium at a distance x_c = 27.5 mm (θ_{endo} = 30°). Note also the sudden acceleration on the epicardium when the cusp reaches the surface in both cases (compare the differences in the spacing of isochrones before and after the breakthrough).

B. Simulated optical signals of intra-myocardial cusp waves

For each of the propagation patterns discussed in the previous section, we calculated optical signals and constructed V^*-maps that reflect the optical upstroke morphology (see Fig. 2). Fig. 4 shows such a V^*-map for a simulation where the cusp wave was at an initial depth of 2 mm below the epicardium (θ_{endo}=30°). Before the cusp reaches the epicardial surface, the wave front has a positive angle with respect to the epicardium and accordingly a low V^* value ≤0.3 (blue) [11]. When the cusp sufficiently approaches the epicardial surface, V^* gradually increases. Finally, after the cusp has disappeared, the wave front shows a negative angle with respect to the epicardial surface and V^* has a value ≥ 0.6 (yellow). Note that V^* changes long before the cusp reaches the surface.

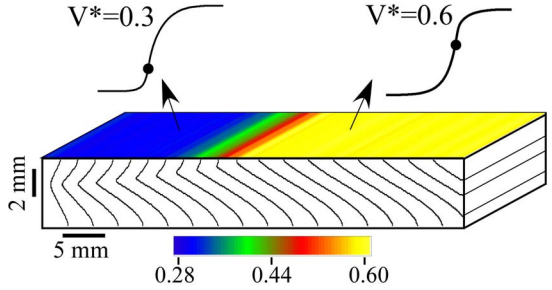

Fig.4. V^*-map of an intra-myocardial cusp. The initial location of the cusp was 2 mm below the epicardial surface (θ_{endo}=30°). Optical action potentials were normalized and V^* was calculated in each pixel of the image. The colors range from blue (low V^*) to yellow (large V^*).

Fig. 5 shows V^* as a function of the cusp's distance from the epicardial surface. V^* remains small as long as the cusp is deep inside the myocardial wall. The influence of the cusp on V^* becomes visible when the cusp reaches a depth of approximately 1 mm. From then on V^* increases linearly until the cusp vanishes at the epicardial surface.

Similar results were obtained for different values of θ_{endo}: cusps affect the optical action potential upstroke and increase the value of V^*, long before they reach the epicardial surface.

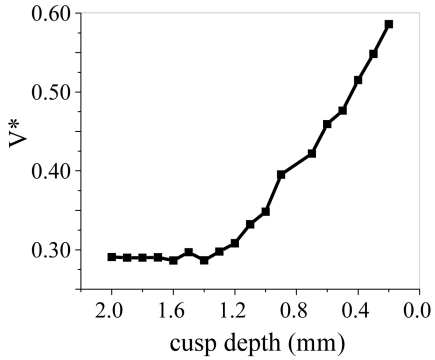

Fig. 5. V^* as a function of the depth of the propagating cusp (θ_{endo}=30°).

C. Experimental recording of a cusp wave

We tested the validity of our simulations experimentally in Langendorff-perfused guinea pig hearts. Earlier computer simulations [19] showed that apical stimulation produces intra-myocardial cusp waves. Here, we test this prediction as well as our method for cusp wave detection using V^*-maps.

Fig. 6A shows an isochronal map of apical stimulation in our experiments. A sudden acceleration of the wave is observed at a distance x_c ~ 8 mm from the apex, typical of an intra-myocardial cusp wave reaching the epicardial surface at the dotted line (compare isochrones in the box with surface isochrones in Fig. 3). Similar patterns were observed in all three hearts.

If the acceleration is indeed caused by a cusp wave, our computational analysis showed that the optical upstroke and V^* should be affected long before the cusp breaks through. Fig. 6B shows the V^*-map corresponding to the activation sequence displayed in Fig. 6A: close to the stimulation site (+), V^* has a value of about 0.2 (blue). At the point where

the cusp reaches the epicardium and the wave starts accelerating (dotted line) V^* has a value of about 0.7 (yellow). However, V^* starts increasing several millimeters before the cusp reaches the epicardial surface. These observations are consistent with our numerical simulations of intra-myocardial cusp waves.

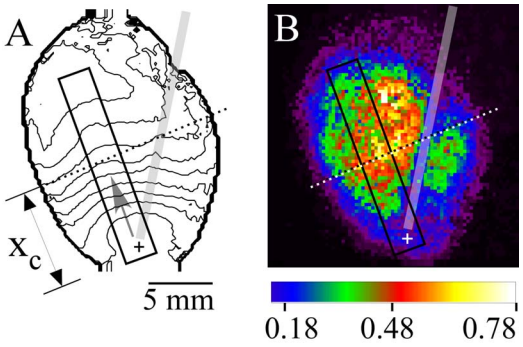

Fig. 6. Optical recording of a cusp wave in an isolated guinea pig heart. The heart was stimulated in the apex (+). The grey shaded area indicates the electrode. Panel A depicts the activation map after ensemble averaging (isochrones at 2 ms intervals). The dotted line indicates the approximate location where the cusp breaks through. The grey arrow indicates the direction of propagation. Compare isochrones in box with surface activation in Fig. 3. Panel B shows the corresponding V^*-map.

IV. Discussion

Optical imaging has become an important tool in the study of cardiac electrical activity [20]. Although optical mapping has mainly been used for surface imaging, recent studies have shown that deeper layers also contribute to the optical signals [10,11]. Specifically, the optical action potential upstroke was found to contain three-dimensional information on the intra-myocardial wave front orientation with respect to the interrogated surface. In the present study, we used this knowledge to detect intra-myocardial cusp waves through their effects on the optical action potential upstroke. We found that the level of maximal upstroke velocity (V^*) changes due to the presence of a cusp in the vicinity of the epicardial surface. Our experimental optical recordings of apical stimulation in isolated guinea pig hearts are consistent with these findings. These results could provide an explanation for the high V^* values that were observed near the base of the ventricles in a computational study of apical stimulation in the whole heart [19].

Acknowledgment

The authors thank R.M. Zaritski for providing computational time on the Montclair cluster (NSF grant CTS-0319555).

References

[1] Clerc, L., Directional differences of impulse spread in trabecular muscle from mammalian heart *J Physiol* , vol. 255, pp. 335-46, Feb, 1976.

[2] Streeter D., *Handbook of Physiology*, pp. 61-112, 1979. American Physiological Society. Bethesda, MD.

[3] Helm, P. A., Tseng, H. J., Younes, L., McVeigh, E. R., and Winslow, R. L., Ex vivo 3D diffusion tensor imaging and quantification of cardiac laminar structure *Magn Reson Med*, vol. 54, pp. 850-9, Oct, 2005.

[4] Sampson, K. J. and Henriquez, C. S., Electrotonic influences on action potential duration dispersion in small hearts: a simulation study *Am J Physiol Heart Circ Physiol*, vol. 289, pp. H350-60, Jul, 2005.

[5] Taccardi, B., Punske, B. B., Sachse, F., Tricoche, X., Colli-Franzone, P., Pavarino, L. F., and Zabawa, C., Intramural activation and repolarization sequences in canine ventricles. Experimental and simulation studies *J Electrocardiol*, vol. 38, pp. 131-7, Oct, 2005.

[6] Panfilov, A. V. and Keener, J. P., Generation of reentry in anisotropic myocardium *J Cardiovasc Electrophysiol*, vol. 4, pp. 412-21, Aug, 1993.

[7] Colli-Franzone, P., Guerri, L., Pennacchio, M., and Taccardi, B., Spread of excitation in 3-D models of the anisotropic cardiac tissue. III. Effects of ventricular geometry and fiber structure on the potential distribution *Math Biosci*, vol. 151, pp. 51-98, Jul, 1998.

[8] Bernus, O., Wellner, M., and Pertsov, A. M., Intramural wave propagation in cardiac tissue: asymptotic solutions and cusp waves *Phys Rev E Stat Nonlin Soft Matter Phys*, vol. 70, pp. 061913Dec, 2004.

[9] Burgess, M. J., Steinhaus, B. M., Spitzer, K. W., and Ershler, P. R., Nonuniform epicardial activation and repolarization properties of in vivo canine pulmonary conus *Circ Res*, vol. 62, pp. 233-46, Feb, 1988.

[10] Hyatt, C. J., Mironov, S. F., Wellner, M., Berenfeld, O., Popp, A. K., Weitz, D. A., Jalife, J., and Pertsov, A. M., Synthesis of voltage-sensitive fluorescence signals from three-dimensional myocardial activation patterns *Biophys J*, vol. 85, pp. 2673-83, Oct, 2003.

[11] Hyatt, C. J., Mironov, S. F., Vetter, F. J., Zemlin, C. W., and Pertsov, A. M., Optical action potential upstroke morphology reveals near-surface transmural propagation direction *Circ Res*, vol. 97, pp. 277-84, Aug 5, 2005.

[12] Faber, G. M. and Rudy, Y., Action potential and contractility changes in Na(+)(i) overloaded cardiac myocytes: a simulation study *Biophys J*, vol. 78, pp. 2392-404, May, 2000.

[13] Bernus, O., Wellner, M., Mironov, S. F., and Pertsov, A. M., Simulation of voltage-sensitive optical signals in three-dimensional slabs of cardiac tissue: application to transillumination and coaxial imaging methods *Phys Med Biol*, vol. 50, pp. 215-29, Jan 21, 2005.

[14] Haskell, R. C., Svaasand, L. O., Tsay, T. T., Feng, T. C., McAdams, M. S., and Tromberg, B. J., Boundary conditions for the diffusion equation in radiative transfer *J Opt Soc Am A Opt Image Sci Vis*, vol. 11, pp. 2727-41, Oct, 1994.

[15] Khait, V., Bernus, O., Mironov, S. F., and Pertsov, A. M., A method for the three-dimensional localization of intra-myocardial excitation centers in cardiac tissue *J. Biomed. Opt.*, vol. 2006.

[16] Bernus, O., Khait, V. D., Wellner, M., Mironov, S. F., and Pertsov, A. M., The forward problem in optical mapping of electrical activity in the heart: application to various imaging methods *Proc. SPIE*, vol. 5696, pp. 13-24, 2005.

[17] Berenfeld, O. and Pertsov, A. M., Dynamics of intramural scroll waves in three-dimensional continuous myocardium with rotational anisotropy *J Theor Biol*, vol. 199, pp. 383-94, Aug 21, 1999.

[18] Matiukas, A., Mitrea, B. G., Pertsov, A. M., Wuskell, J. P., Wei, M. D., Watras, J., Millard, A. C., and Loew, L. M., New Near Infrared Optical Probes of Cardiac Electrical Activity *Am J Physiol Heart Circ Physiol*, vol. Jan 6, 2006.

[19] Bishop, M. J., Rodriguez, B., Eason, J., Whiteley, J. P., Trayanova, N., and Gavaghan, D. J., Synthesis of voltage-sensitive optical signals: application to panoramic optical mapping *Biophys J*, vol. 90, pp. 2938-45, Apr, 2006.

[20] Efimov, I. R., Nikolski, V. P., and Salama, G., Optical imaging of the heart *Circ Res*, vol. 95, pp. 21-33, Jul 9, 2004.

[21] Baxter, W. T., Mironov, S. F., Zaitsev, A. V., Jalife, J., and Pertsov, A. M., Visualizing excitation waves inside cardiac muscle using transillumination *Biophys J*, vol. 80, pp. 516-30, Jan, 2001.